Spatially Adaptive 3D Inverse for Optical Sectioning

Dmitriy Paliy[a], Vladimir Katkovnik[b], Karen Egiazarian[c]

Tampere International Center for Signal Processing, Tampere University of Technology,
P.O.Box 553, FIN-33101 Tampere, FINLAND.
[a]dmitriy.paliy@tut.fi, [b]katkov@cs.tut.fi, [c]karen.egiazarian@tut.fi

ABSTRACT

In this paper, we propose a novel nonparametric approach to reconstruction of three-dimensional ($3D$) objects from $2D$ blurred and noisy observations which is a problem of computational optical sectioning. This approach is based on an approximate image formation model which takes into account depth varying nature of blur described by a matrix of shift-invariant $2D$ point-spread functions (PSF) of an optical system. The proposed restoration scheme incorporates the matrix regularized inverse and matrix regularized Wiener inverse algorithms in combination with a novel spatially adaptive denoising. This technique is based on special statistical rules for selection of the adaptive size and shape neighbourhood used for the local polynomial approximation of the $2D$ image intensity. The simulations on a phantom $3D$ object show efficiency of the developed approach. The objective result evaluation is presented in terms of quadratic-error criteria.

Keywords: $3D$ inverse, adaptive denoising, optical sectioning

1. INTRODUCTION

One can see well only the focused areas of a $3D$ object, observing it in a microscope or another optical device, while others are seen as blurred. However, these out-of-focus structures are in the field of view and thus obscure those which are in-focus. Different areas appear in focus by moving the object along the optical axis. The problem arises as a reconstruction of a true $3D$ object from a set of $2D$ observations. A series of images acquired for different positions of an observed object or focus of a camera is used widely in image processing and computer vision. The typical areas are the computational optical sectioning,[1,2] estimation of depth from focus or defocus,[3] all-in-focus or arbitrary-view image generation,[4] etc.

In general, images suffer from degradation due to the out-of-focused areas contributing to the in-focus areas. For instance, in a process of specimen observation in a microscope there is only one portion that appears in focus. However, usually a specimen is not flat but $3D$ structure. Therefore, some portions are out of focus. Nevertheless, these out-of-focus structures are in the field of view and thus obscure the in-focus plane. In order to obtain a deblurred $3D$ image of a specimen, it is common to use a method called optical sectioning. The microscope is focused at a given focal plane and the image is recorded. This image is an optical slice. Then, the microscope is refocused and another image is recorded. This process is repeated until the whole specimen is covered.[2] The restoration of the same scene from multiple degraded observations is typical for macro-world also, which is often classified as a multichannel image restoration problem. Usually, this problem exploits methods of a single-image restoration to degraded multi-channel images to recover the original scene.[4] The $3D$ optical sectioning equipped with digital deblurring algorithms is a powerful modern tool for visualization of specimens in biology, medicine, mineralogy, etc. Computational restoration methods applied to slice images are quite an efficient and perspective tool.

The $3D$ PSF is the main factor describing how a point source of light is being distributed laterally and across the focal planes. It plays a crucial role in image formation and its reconstruction. $3D$ inverse is a problem of object restoration from its observations using a known PSF of optical system. It is an ill-posed problem.[5] It means that small perturbations in initial data (observed image and inaccuracy in the used PSF model) result in large changes in the solution. For solving the deconvolution problem with a given PSF a number of approaches were proposed since the mid 1970s under various idealizations of the PSF and noise model.

Send correspondence to Dmitriy Paliy. E-mail: dmitriy.paliy@tut.fi

In microscopy there are two approaches to reduce out-of-focus contributions: optical and computational. In the optical approach a confocal microscope is used that reduces the contribution from the out-of-focus fluorescence. The recorded clearer focal plane images are an optical equivalent of a series of microtome slices allowing a $3D$ reconstruction of a specimen.

In the computational approach, image processing is applied to process the set of $2D$ optical slices in order to reduce the out-of-focus interferences. This method is based on information about the processes of image formation. The most severe degradation is often caused by diffraction at objective and condenser lenses. This degradation is modeled by the PSF of the microscope optical system.

Image deconvolution has become an established technique to improve both resolution and signal-to-noise ratio of serially sectioned three-dimensional images.[1] The reconstruction of $3D$ objects by means of optical sectioning is very popular in fluorescence microscopy imaging. A number of techniques was proposed for optical sectioning based on the iterative expectation-maximization approach.[2,6] Using the expectation-maximization formalism, algorithms for maximum-likelihood image restoration were developed using a depth-variant model for the optical sectioning microscopy. Theoretical analysis of properties for proposed techniques is an advantage. However, these methods are efficient but computationally expensive. Another works which exploit iterative inverse schemes, can be seen also in.[7,8]

The iterative solution presented by a combination of the conjugate gradient method with the Tikhonov regularization is proposed in.[1] The conjugate gradient iteration scheme was used considering either Gaussian or Poisson noise models. For the regularization, the standard Tikhonov method was modified. However, the generic design of the algorithm allows for more regularization approaches. To determine the regularization parameter, the generalized cross-validation method is used. Tests produced for both simulated and experimental fluorescence wide-field data show reliable results.

Linear non-iterative methods for deconvolution of $3D$ images in computational optical sectioning microscopy are proposed in.[9] The authors consider also Gaussian and Poissonian noise formation models. An approach using complex-valued wavelet transform to obtain extended depth-of-focus for multi-channel microscopy images is proposed in.[10] However, this method does not take into account the image acquisition model.

Knowledge about image formation is an important issue in the restoration techniques. The PSF of an optical system as the main factor plays a crucial role. In this paper we assume that the PSF is known a priory. For example, modeling and estimation of PSF are done in[2,13] for optical system of a microscope or in[4] for a photocamera. The reconstruction of all-in-focus image from two arbitrarily focused images is proposed in.[4] The true scene is supposed to have the background and foreground regions only. The authors propose a method for PSF estimation from degraded observed images and use the inverse filter to obtain an original scene. However, the image formation model does not assume a presence of noise.

In this paper we focus on the noniterative method of reconstruction and generalize the spatially adaptive $2D$ deblurring algorithm developed in[11] to the $3D$ imaging. It incorporates the regularized inverse and regularized Wiener filters. The noise model considered in this paper is Gaussian. The scale-adaptive denoising technique is used to remove it effectively.

The simulations done for a complex phantom image show the efficiency of the proposed technique.

We begin paper by the problem setting in Section 2. Then, the proposed technique for inversion and denoising steps is given in Section 3. Finally, in Section 4 we discuss implementation aspects and show simulation results.

2. PROBLEM STATEMENT

Mathematically a variety of image capturing principles can be described by the Fredholm integral of the first kind in $3D$ space $z(x) = \int v(x,t)y(t)dt$, where $x, t \in \mathbb{R}^3$, $v(t)$ is a $3D$ PSF of a system, $y(t)$ is a function of a real $3D$ object and $z(x)$ is an observed signal.[8,12] In general, PSF v is varying in all dimensions. A natural simplification is the assumption that it is shift-invariant which leads to a process formation by a convolution operation. When noise is involved, the observation model is

$$z(x) = (v \circledast y)(x) + \varepsilon(x), \tag{1}$$

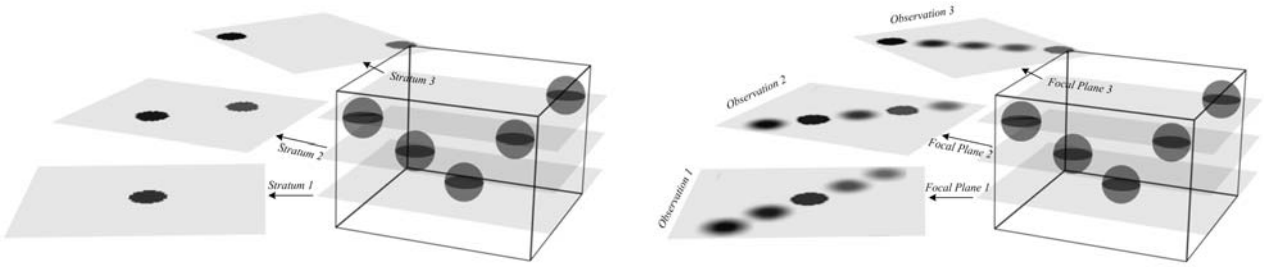

a) b)

Figure 1. $3D$ object consisted of 5 spheres: a) strata of the object; b) observation of each stratum focusing preciselly at stratum 1, stratum 2, and stratum 3.

where " $\circledast$ " denotes a $3D$ convolution operation and $\varepsilon(x)$ is a noise.

In the continuous frequency domain the model (1) takes the form:

$$Z(\omega) = V(\omega) \cdot Y(\omega) + \varepsilon(\omega), \tag{2}$$

where $Z(\omega) = \mathcal{F}\{z(x)\}$, $\omega \in \mathbb{R}^3$, i.e. $\omega = (\omega_1, \omega_2, \omega_3)$, is a representation of the signal z in the Fourier domain and $\mathcal{F}\{\cdot\}$ denotes a Fourier transform (FT), $V(\omega) = \mathcal{F}\{v(x)\}$, $Y(\omega) = \mathcal{F}\{y(x)\}$, $\varepsilon(\omega) = \mathcal{F}\{\varepsilon(x)\}$.

The assumption that the PSF is shift-invariant in all three dimensions usually does not correspond to reality. A more natural assumption is that the PSF is shift-invariant in (x_1, x_2) plane and varying in the third dimension x_3.[2,6,17] This approach leads to the optical sectioning formalism originated in digital microscopy and astronomy.

According to this technique the optical system is focused at some focal plane and an image is recorded, then it is focused at another plane and another image is recorded, and so on. The focusing planes may differ from the planes of interests. Precise focusing is not needed for reconstruction. However, the spatial resolution depends on a number of recorded images.

Suppose that we wish to reconstruct a $3D$ image intensity function $y(x)$, $x \in \mathbb{R}^3$, from its blurred and noisy observation $z(x)$. In the argument $x = (x_1, x_2, x_3)$ the first two variables x_1 and x_2 define the pixel's coordinates of $2D$ image obtained from $y(x)$ with the fixed depth coordinate x_3. The axe x_3 is parallel to the optical axe of the optical system and perpendicular to the 2D image plane.

We consider the discrete observation model in the following form:

$$z_i(\tilde{x}) = \sum_{j=1}^{m} (v_{i,j} \circledast y_j)(\tilde{x}) + \varepsilon_i(\tilde{x}),\ i = 1, ..., n, \tag{3}$$

where $\tilde{x} \in \mathbb{R}^2$, $\tilde{x} = (x_1, x_2)$, i is a discrete variable used for the depth variable x_3, and $\mathbf{v} = (v_{i,j})$ is an $n \times m$ matrix of the $2D$ $PSFs$. PSF $v_{i,j}$ corresponds to the observation of the object slice j from focusing at the position i. ε_i is a white zero-mean Gaussian noise with variance σ_i^2, $i = 1, ..., n$.

It is required to restore the $3D$ image (the slices of the object, which is described by $\mathbf{y}(\tilde{x}) = (y_1(\tilde{x}), ..., y_m(\tilde{x}))$) from n blurred $2D$ projections $\mathbf{z}(\tilde{x}) = (z_1(\tilde{x}), ..., z_n(\tilde{x}))$. Here, m is a number of physical slices of the object taken into consideration.

Let $Z_i(\widetilde{\omega})$ be the discrete $2D$ Fourier transform of $z_i(\tilde{x})$, $Z_i(\widetilde{\omega}) = \mathcal{F}\{z_i(\tilde{x})\}$. Here $\widetilde{\omega} \in \{(\omega_1, \omega_2),\ \omega_i = 0, 1, ..., n_i - 1,\ i = 1, 2\}$ is the $2D$ normalized discrete frequency. Then, equation (3) in the frequency domain can be written as follows:

$$\begin{pmatrix} Z_1 \\ ... \\ Z_n \end{pmatrix} = \begin{pmatrix} V_{11} & ... & V_{1m} \\ ... & ... & ... \\ V_{n1} & ... & V_{nm} \end{pmatrix} \begin{pmatrix} Y_1 \\ ... \\ Y_m \end{pmatrix} + \begin{pmatrix} \varepsilon_1 \\ ... \\ \varepsilon_n \end{pmatrix}, \tag{4}$$

where $V_{ij}(\widetilde{\omega}) = \mathcal{F}\{v_{ij}(\tilde{x})\}$, $Y_j(\widetilde{\omega}) = \mathcal{F}\{y_j(\tilde{x})\}$, and $\varepsilon_i(\widetilde{\omega}) = \mathcal{F}\{\varepsilon_i(\tilde{x})\}$.

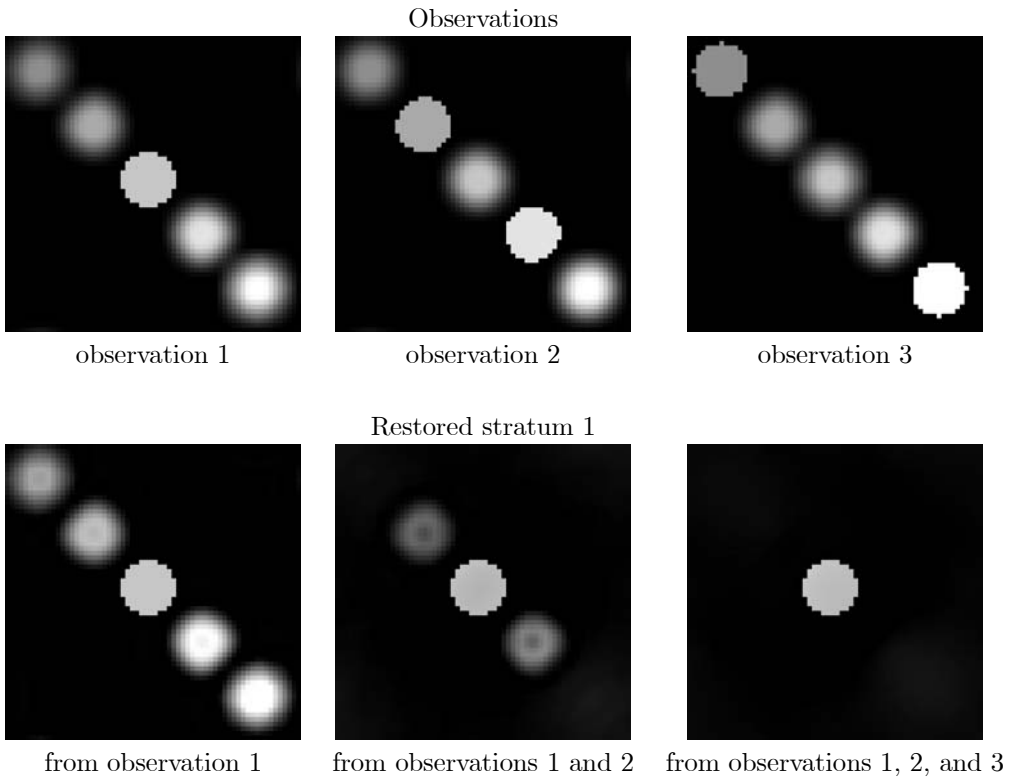

Figure 2. Example of reconstruction from noise-free observations of the object showed in Fig. 1. First row is the observations of stratum 1, 2, and 3 consiquently from left to right focusing precisely at each stratum. Second row is the examples of restoration of the stratum 1 from observation 1, observations 1 and 2, and from all 3 observations consiquently from left to right.

Finally, the collected $3D$ observation $\mathbf{Z} = (Z_1, ..., Z_n)^T$ is a set of blurred $2D$ images. In order to find the true object $\mathbf{Y} = (Y_1, ..., Y_m)^T$ we need to solve the system of linear equations (4).

We obtain for (4) the following vector-matrix representation defined in the $2D$ frequency domain:

$$\mathbf{Z}(\widetilde{\omega}) = \mathbf{V}(\widetilde{\omega})\mathbf{Y}(\widetilde{\omega}) + \boldsymbol{\varepsilon}(\widetilde{\omega}). \tag{5}$$

The equations (2) and (5) are similar but the difference is essential. The continuous model (2) is assumed to be shift-invariant in all three dimensions including x_3 particularly. On the contrary, the model (5) is shift-invariant in the plane $\widetilde{x} = (x_1, x_2)$ and can be shift-varying in x_3.

The method feasibility depends on the properties of the $n \times m$ matrix $\mathbf{V} = (V_{ij})$. An ill-posedness of restoration problem arises from small singular values of $\mathbf{V}(\widetilde{\omega})$ which after inversion would cause noise amplification. This is what makes the problem of restoration of $\mathbf{Y}(\widetilde{\omega})$ from $\mathbf{Z}(\widetilde{\omega})$ ill-posed. Different restoration techniques cope with it in a different way.

Fig.1 illustrates the setting of the problem. The $3D$ object consists of 5 spheres. The object slices call *strata*[2] lie in the planes perpendicular to the optical axe. It is assumed that the thickness of the strata is small and variation of the PSF with respect to the coordinate x_3 in one stratum is insignificant. The object in Fig.1 is discretized to $m = 3$ strata. In observations of this object one can see clearly only the strata which are in the focal planes while others are blurred (Fig.1b). The aim is to reconstruct the original strata Fig.1a from their $n = 3$ observations Fig.1b.

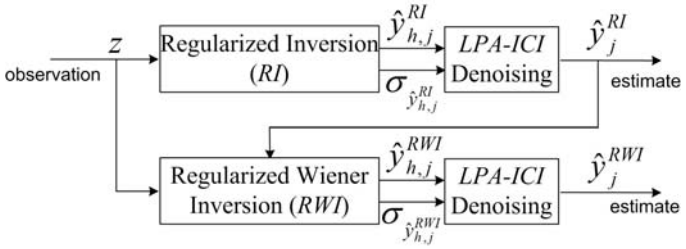

Figure 3. The proposed restoration scheme includes RI step with adaptive LPA-ICI denoising in order to obtain a reference signal for the RWI filter.

3. PROPOSED TECHNIQUE

We develop the technique which is a vector-matrix generalization of the regularized inverse (RI) and regularized Wiener inverse (RWI) adaptive scale deblurring algorithms proposed in.[11,15] The intersection of confidence intervals (ICI) rule[14] is exploited for the adaptive scale filtering of the reconstructed $2D$ slices of the $3D$ object function $\mathbf{y}(\tilde{x})$. The algorithm consists of two stages. At the first stage the RI filter and adaptive local polynomial approximation (LPA) with the ICI rule are used in order to obtain the estimate $\hat{\mathbf{y}}^{RI}(\tilde{x})$ exploited at the second stage as a reference signal. The second stage incorporates the RWI filter and LPA-ICI to obtain the final result $\hat{\mathbf{y}}^{RWI}(\tilde{x})$ (Fig. 3).

3.1. Regularized Inverse

The RI filter is obtained by minimization of the penalized quadratic residual function which for the problem (5) is given in the form:

$$\begin{aligned} \mathbf{J} &= \|\mathbf{Z}(\widetilde{\omega}) - \mathbf{V}(\widetilde{\omega})\mathbf{Y}(\widetilde{\omega})\|_2^2 + r_1^2 \|\mathbf{Y}(\widetilde{\omega})\|_2^2 = \\ &= \sum_{\widetilde{w}} (\mathbf{Z}(\widetilde{\omega}) - \mathbf{V}(\widetilde{\omega})\mathbf{Y}(\widetilde{\omega}))^H (\mathbf{Z}(\widetilde{\omega}) - \mathbf{V}(\widetilde{\omega})\mathbf{Y}(\widetilde{\omega})) + r_{RI}^2 \sum_{\widetilde{w}} \mathbf{Y}^H(\widetilde{\omega})\mathbf{Y}(\widetilde{\omega}), \end{aligned} \tag{6}$$

where r_{RI}^2 is a regularization parameter and "^{H}" denotes the Hermitian transpose.

The minimum of $\mathbf{J}$ is achieved when $\partial \mathbf{J}/\partial \mathbf{Y}^H = 0$. Calculation of this derivative gives the estimate:

$$\widehat{\mathbf{Y}}^{RI}(\widetilde{\omega}) = (\mathbf{V}^H(\widetilde{\omega})\mathbf{V}(\widetilde{\omega}) + r_{RI}^2 \mathbf{I}_{m\times m})^{-1} \mathbf{V}^H(\widetilde{\omega})\mathbf{Z}(\widetilde{\omega}), \tag{7}$$

where $\mathbf{I}_{m\times m}$ is the $m \times m$ identity matrix.

Following the technique developed in[11,15] we introduce the filtered RI estimate as follows:

$$\widehat{\mathbf{Y}}_h^{RI}(\widetilde{\omega}) = G_h(\widetilde{\omega})\widehat{\mathbf{Y}}^{RI}(\widetilde{\omega}), \tag{8}$$

where G_h is a low-pass filter generated by LPA. This filter is the same for all components of the vector $\widehat{\mathbf{Y}}^{RI}(\widetilde{\omega})$.

Here, h is an important scale-parameter of the filter which is *selected adaptively* by the ICI rule. In spacial domain $\hat{y}_{h,j}^{RI}(\tilde{x}) = \mathcal{F}^{-1}\left\{\hat{Y}_{h,j}^{RI}(\widetilde{\omega})\right\}$, $j = 1, ..., m$. The idea and use of the LPA-ICI is described later.

Using formulas (5), (7), (8), and Parseval's theorem the variance at every point of the estimate $\hat{y}_{h,j}^{RI}(\tilde{x})$, $j = 1, ..., m$, is computed as

$$\sigma^2_{\hat{y}^{RI}_{h,j}(\tilde{x})} = var\{\hat{y}_{h,j}^{RI}(\tilde{x})\} = \frac{1}{n_1 n_2} \sum_{\widetilde{w}} (\mathbf{Q}_{RI}(\widetilde{\omega})\boldsymbol{\sigma}^2 \mathbf{Q}_{RI}^H(\widetilde{\omega}))_{j,j},\ j = 1, ..., m. \tag{9}$$

Here, $\mathbf{Q}_{RI}(\widetilde{\omega})$ is a transfer matrix of (8)

$$\mathbf{Q}_{RI}(\widetilde{\omega}) = G_h(\widetilde{\omega})(\mathbf{V}(\widetilde{\omega})^H \mathbf{V}(\widetilde{\omega}) + r_{RI}^2 \mathbf{I}_{m\times m})^{-1} \mathbf{V}^H(\widetilde{\omega})$$

and $\boldsymbol{\sigma}^2 = diag(\sigma_1^2, ..., \sigma_n^2)$ is a diagonal matrix of the variances of observations $\mathbf{z}(\tilde{x}) = (z_1(\tilde{x}), ..., z_n(\tilde{x}))$.

The variance of noise for every observation can be different. The variances $\left(\sigma^2_{\hat{y}^{RI}_{h,j}(\tilde{x})}\right)$ are used in the ICI rule for the adaptive selection of the scale h.

3.2. Regularized Wiener Inverse

Looking for an optimal linear estimate $\hat{y}_j(\tilde{x}) = (q^{WI}_{j,i} \circledast z_i)(\tilde{x})$, $i = 1, ..., n$, $j = 1, ..., m$, of a smoothed signal $y_{h,j}(\tilde{x}) = (g_h \circledast y_j)(\tilde{x})$ we come to the Wiener inverse filter $\mathbf{Q}_{WI} = \left(\mathcal{F}\{q^{WI}_{j,i}\}\right)$ by minimizing criterion function

$$\mathbf{J} = E\left\{\left\|\mathbf{Y}_h(\widetilde{\omega}) - \widehat{\mathbf{Y}}(\widetilde{\omega})\right\|_2^2\right\} = E\left\{\|G_h(\widetilde{\omega})\mathbf{Y}(\widetilde{\omega}) - \mathbf{Q}_{WI}(\widetilde{\omega})\mathbf{Z}(\widetilde{\omega})\|_2^2\right\}.$$

Solution of $\partial\mathbf{J}/\partial\mathbf{Q}^H_{WI} = 0$ gives us the transfer matrix for the Wiener filter:

$$\mathbf{Q}_{WI} = G_h\mathbf{Y}\mathbf{Y}^H\mathbf{V}^H(\mathbf{V}\mathbf{Y}\mathbf{Y}^H\mathbf{V}^H + n_1n_2\boldsymbol{\sigma}^2)^{-1}. \tag{10}$$

Inserting the regularization parameter r^2_{RWI} into (10) we obtain the regularized Wiener inverse (RWI) filter:

$$\mathbf{Q}_{RWI} = G_h\mathbf{Y}\mathbf{Y}^H\mathbf{V}^H(\mathbf{V}\mathbf{Y}\mathbf{Y}^H\mathbf{V}^H + n_1n_2r^2_{RWI}\boldsymbol{\sigma}^2)^{-1}. \tag{11}$$

The filtered RWI estimate similarly to the (8) has the following form:

$$\widehat{\mathbf{Y}}^{RWI}_h(\widetilde{\omega}) = \mathbf{Q}_{RWI}(\widetilde{\omega})\mathbf{Z}(\widetilde{\omega}). \tag{12}$$

In spacial domain $\hat{y}^{RWI}_{h,j}(\tilde{x}) = \mathcal{F}^{-1}\left\{\hat{Y}^{RWI}_{h,j}(\widetilde{\omega})\right\}$, $j = 1, ..., m$. The variances for the estimate (12) are:

$$\sigma^2_{\hat{y}^{RWI}_{h,j}(\tilde{x})} = var\{\hat{y}^{RWI}_{h,j}(\tilde{x})\} = \frac{1}{n_1n_2}\sum_{\widetilde{w}}(\mathbf{Q}_{RWI}(\widetilde{\omega})\boldsymbol{\sigma}^2\mathbf{Q}^H_{RWI}(\widetilde{\omega}))_{j,j},\ j = 1, ..., m, \tag{13}$$

and they are used in the following $LPA - ICI$ post-processing.

3.3. LPA-ICI Denoising

The LPA-ICI algorithm is a scale-adaptive denoising technique developed in.[11,14–16] The LPA is a tool for linear filter design. In particular, the smoothing filter G_h in (8) and (12) is obtained by LPA. This filter is used with varying scales (window sizes) h.

The ICI rule is the algorithm for the window size selection for every point $\widetilde{x}$. The idea of this approach is as follows. The algorithm searches for a largest local vicinity of the point of estimation where the LPA assumption fits well to the data. The estimates $\widehat{y}_{h,j}(\tilde{x})$, $j = 1, .., m$, are calculated for a grid of window sizes (scales) $h \in H = \{h_1, h_2, ..., h_J\}$, where $h_1 < h_2 < ... < h_J$. The adaptive scale is defined as the largest h^+ of those windows in the set H which estimate does not differ significantly from the estimators corresponding to the smaller window sizes. This general idea is implemented as follows. We consider a sequence of confidence intervals $D_k = \left[\widehat{y}_{h_k,j}(\tilde{x}) - \Gamma\sigma_{\hat{y}_{h_k,j}(\tilde{x})}, \widehat{y}_{h_k,j}(\tilde{x}) + \Gamma\sigma_{\hat{y}_{h_k,j}(\tilde{x})}\right]$, $k = 1, .., J$, where $\Gamma > 0$ is a parameter and $\sigma_{\hat{y}_{h_k,j}(\tilde{x})}$ is a standard deviation of estimate. The ICI rule can be stated as follows: *consider the intersection of the confidence intervals* $I_k = \bigcap_{i=1}^k D_i$ *and let* k^+ *be the largest of the indices* k *for which* I_k *is non-empty. Then the optimal scale* h^+ *is defined as* $h^+ = h_{k^+}$ *and, as result, the optimal scale estimate is* $\widehat{y}_{h^+,j}(\tilde{x})$. The standard deviations $\sigma_{\hat{y}_{h_k,j}(\tilde{x})}$ of estimates are computed according to Eq. (9) and (13).

Theoretical analysis produced in[18] for $1D$ case shows that this adaptive scale gives the best possible pointwise mean-squared error. *In practice this means that adaptively, for every pixel,* ICI *allows the maximum degree of smoothing, stopping before oversmoothing begins.*[19]

The parameter Γ is a key element of the algorithm as it says when the difference between the estimates is large or small. Too large value of this parameter leads to signal oversmoothing and too small value leads to undersmoothing. The reasonable value to preserve a signal and remove noise as mush as possible is somewhere between.

Selection of Γ can be obtained from some heuristic and theoretical considerations (e.g.[11,14,15,20]). In this paper we treat Γ as a fixed design parameter.

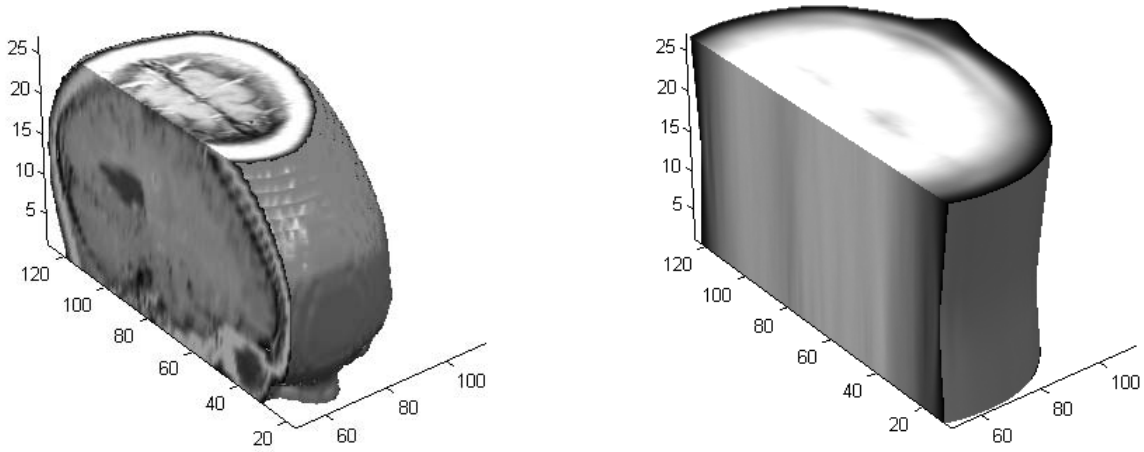

Figure 4. The phantom $3D\ MRI$ object used in simulations: a) A subvolume of the true object; b) A corresponding subvolume of blurred and noisy observations.

4. EXPERIMENTS

4.1. PSF simulation

The knowledge about a PSF and its properties is very important in reconstruction techniques. There is a variety of commercial products to simulate or to measure a real PSF. We assume that the PSF is given a priori and has a Gaussian form: $v(x) = \frac{1}{\sqrt{2\pi}\sigma_{x_1}} \exp\left(-\frac{x_1^2}{2\sigma_{x_1}^2}\right) \cdot \frac{1}{\sqrt{2\pi}\sigma_{x_2}} \exp\left(-\frac{x_2^2}{2\sigma_{x_2}^2}\right) \cdot \frac{1}{\sqrt{2\pi}\sigma_{x_3}} \exp\left(-\frac{x_3^2}{2\sigma_{x_3}^2}\right)$. It is assumed that standard deviations of the Gaussian PSF in planes perpendicular to optical axe are equal $\sigma_{x_1} = \sigma_{x_2} = \sigma_{xy}$ and depend on x_3. With respect to x_3 function $v(x)$ has a constant standard deviation $\sigma_{x_3} = \sigma_z$. So, $PSFs$ used in (3) are:

$$v_{i,j}(x_1, x_2) = \frac{1}{2\pi\sigma_{xy}^2(x_3(i) - x_3(j))} \exp\left(-\frac{x_1^2 + x_2^2}{2\sigma_{xy}^2(x_3(i) - x_3(j))}\right) \cdot \frac{1}{\sqrt{2\pi}\sigma_z} \exp\left(-\frac{(x_3(i) - x_3(j))^2}{2\sigma_z^2}\right), \qquad (14)$$

where $i = 1, ..., n$, $j = 1, ..., m$.

The value of σ_z is important because it is directly related to the conditioning of the matrix $(v_{i,j})$, i.e. with the ability to solve the system of equations (4). Physically, it shows how strong a contribution of the jth stratum to the observation at ith focal plane is. When $\sigma_z \to 0$ the observation $z_i(\widetilde{x})$ consists only of the stratum at focus $y_j(\widetilde{x})$ $(i = j)$ and there is no need to make an inversion. On the other hand, when $\sigma_z \to \infty$ the observations consist of all strata which are blurred and equally visible. In this case, reconstruction is *impossible* even in a noise-free case. In all experiments σ_z is fixed to the value 15.

In simulations σ_{xy} depends on the distance between focal plane i and stratum j as follows:

$$\sigma_{xy} = k\,|x_3(i) - x_3(j)|\,, \qquad (15)$$

where $k > 0$ is a coefficient. This model means that the stratum blur is larger for the strata located further from the plane of focusing.

The PSFs are normalized in such a way that $\sum_{j=1}^{m} \sum_{\widetilde{x}} v_{i,j}(\widetilde{x}) = 1$.

In practice σ_z and σ_{xy} are usually variable because of imperfection of optics and other physical phenomena. In this paper, according to (15), we assume that σ_{xy} is a constant for a fixed $|x_3(i) - x_3(j)|$.

	Test A		Test B		Test C	
	RMSE	**PSNR**	**RMSE**	**PSNR**	**RMSE**	**PSNR**
RI	0.1180	18.73	0.1376	17.38	0.1032	19.94
RI with $LPA-ICI$	0.1038	19.85	0.1267	18.18	0.0861	21.50
RWI	0.1035	19.87	0.1272	18.15	0.0864	21.46
RWI with $LPA-ICI$	0.1010	20.05	0.1238	18.44	0.0849	21.64

Table 1. Average $RMSE$ and $PSNR$ (dB) values given in columns named 'Test A', 'Test B', and 'Test C', obtained for the proposed technique for Tests A, B, and C, respectively.

4.2. Noise Level

We use a blurred signal-to-noise ratio ($BSNR$) for evaluation of the level of the noise in experiments:

$$BSNR_i = 10\log_{10}\left(\frac{\left\|\sum_j (v_{i,j} \circledast y_j)(\tilde{x}) - \frac{1}{\#}\sum_{\tilde{x}}\left(\sum_j (v_{i,j} \circledast y_j)(\tilde{x})\right)\right\|_2^2}{n_1 n_2 \sigma_i^2}\right),$$

where $i = 1, ..., n$ and $j = 1, ..., m$.

In estimation and filtering we assume that the level of the noise is unknown and estimated (see algorithms in[21, 22]).

4.3. Results

In this section we present simulation results illustrating a performance of the developed technique.

One of the models used in the experiments is shown in Fig.1. A $3D$ object consists of 5 nonoverlapping spheres. A simplified discrete model of this object is given by 3 strata shown in Fig.1a. Observations are produced by focusing the optical system on each stratum Fig.1b. These three $2D$ observation-images are used for reconstruction of the images in the three strata. The reconstruction results are given in Fig.2. It is assumed that the observations are noiseless and the pure inverse procedure is used. It means that no denoising is applied and only the RI algorithm is used with $r_{RI} = 0$.

The left image in the second row of Fig.2 shows reconstruction of the stratum 1 from the observations obtained from a single observation-image corresponding to focusing precisely at the stratum 1 (focal plane 1). Naturally, this reconstruction is identical to the observation-image shown in the first row of this figure (left). Thus, the stratum 1 is in focus while the strata 2 and 3 are blurred.

The middle image of the second row shows the reconstruction of the same stratum 1 done from the observations of strata 1 and 2. It is seen that the interference of planes 2 and 3 is lower in this reconstruction. The right image of the second row demonstrates the perfect reconstruction of the stratum 1. This result is obtained using for reconstruction all three observation-images 1, 2, and 3. The experiment confirms that the algorithm gives perfect reconstruction when sufficient number of observations is available and there is no noise.

A second group of experiments concerns noisy data and demonstrates how a redundancy of observations allows to filter data and reduce a strong interference of different images.

As a complex phantom we use a $3D$ body modeling an MRI datascan of a human cranium. This numerical model is available within MATLAB. The image file *mri.tif* presents 27 slices of 128×128 cross-section images of a cranium. We use this model in order to imitate observation data for the considered 3D inverse imaging. Intensity values are in the range from 0 to 1, $y_j(\tilde{x}) \in [0, 1]$. It consists of 27 object slices enumerated from 1 to 27, $x_3(j) = j$, $j = 1, ..., 27$. A corresponding subvolume of the true object is visualized in Fig.4a. A subvolume of 27 noisy and blurred observations is shown in Fig.4b as they are recorded by focusing one after another at each object slice.

We set the additive noise variances σ_i^2 in such a way that $BSNR \simeq 40$ dB, which is significant level of the noise for this sort of problems. It is strongly visible on the reconstructed by RI technique strata (e.g. Fig.5c). The adaptive $LPA-ICI$ technique is exploited to remove it.

The directional LPA convolution kernels of the zero-order are applied for the filters in (8) and (12). We use 8 sectorial directional kernels with the window lengths defined by the set $H_1 = \{1, 3, 5, 9, 17\}$ and the window width defined by the set $H_2 = \{1, 1, 1, 2, 2\}$.

The developed algorithm can be used with and without the $LPA-ICI$ filtering. Regularization parameters for the RI and RWI algorithms without $LPA-ICI$ are fixed as follows: $r_{RI} = 0.00001$ and $r_{RWI} = 0.006$. For the RI and RWI algorithms with the $LPA-ICI$ filtering we use smaller values of the rugularization parameters equal to $r_{RI}/6$ and $r_{RWI}/6$.

In all cases the parameter Γ is fixed to be $\Gamma = 1$ and $\Gamma = 2$ for RI and RWI algorithms, respectively.

The criteria used to evaluate the algorithm performance are the square root mean squares error ($RMSE$)

$$RMSE_j = \sqrt{\frac{1}{n_1 n_2} \sum_{\tilde{x}} \left(y_j(\tilde{x}) - \hat{y}_j(\tilde{x})\right)^2},$$

and peak signal-to-noise ratio ($PSNR$)

$$PSNR_j = 10 \log_{10} \left(\frac{\max_{\tilde{x}}(y_j(\tilde{x}))^2}{\frac{1}{n_1 n_2} \sum_{\tilde{x}} \left(y_j(\tilde{x}) - \hat{y}_j(\tilde{x})\right)^2} \right),$$

where j numbers the reconstructed image in the strata.

The $2D$ strata $y_j(\tilde{x})$ of the true MRI object are shown in Fig.5a for $j = 1 + \triangle k$, where $\triangle = 3$ and $k = 0, ..., 8$, ordered from the left to right and top to bottom. The $2D$ blurred noisy observations $z_i(\tilde{x})$ of these strata are illustrated in Fig.5b, by focusing precisely at positions j, i.e. $i = j$.

In experiments we run the following tests in order to reconstruct the true object strata shown in Fig.5a:

Test A: Let the observations $z_i(\tilde{x})$ consist of 9 strata $y_j(\tilde{x})$, $j = 1 + \triangle k$, where $\triangle = 3$ and $k = 0, ..., 8$, of the MRI object by focusing precisely at the positions j, i.e. $i = j$. Applying the proposed technique, we reconstruct this object at positions j. The results of the RI reconstruction only are shown in Fig.5c. The slices are reconstructed and the object is clearly visible but the noise is significant. The average $RMSE$ and $PSNR$ values over these 9 images are given in Table 1 in the 'Test A' column and row 'RI'.

The adaptive $LPA-ICI$ denoising technique significantly improves the quality of reconstruction visually and numerically. It can be seen in Fig.5d where the images after the RWI reconstruction with the $LPA-ICI$ filtering are shown. The level of noise is less and smaller details are better preserved. The average results over 9 images of numerical evaluations are given in Table 1 in the 'Test A' column and 'RWI with $LPA-ICI$' row. It illustrates a successive performance improvement caused by the $LPA-ICI$ filtering as well as using the RWI instead of the simpler RI algorithm.

Test B: In practice, a real object (a scene of observation) consists of infinite number of physical strata and observer can register only a part of them. Thus, let us assume that the positions i of observations $z_i(\tilde{x})$ are shifted with respect to the positions of the targeted strata. The coordinates of the observations are given as $i = 14 + \triangle k$, where $\triangle = 3$ and $k = 0, ..., 8$. These observations are used for reconstruction of the targeted strata $y_j(\tilde{x})$, $j = 1 + \triangle k$, shown in Fig.5a. It means that the strata $y_j(\tilde{x})$ at the positions $j = 1, 4, .., 10$ are always out of focus. The result of restoration by RWI with the $LPA-ICI$ denoising is shown in Fig.5e and average numerical criteria values are given in Table 1 column 'Test B'. It is seen that one part of the object, which is covered by observation, is well reconstructed (Fig.5e bottom-right image) while other has a lot of image artefacts (Fig.5e top-left image).

Test C: In the last test we show the influence of a larger number of observations on the quality of restoration. In this test we assume that the true object consists of 9 strata the same as in the Test A. However, the number of observations is larger. The coordinates of the observations are $i = 1 + \triangle k$, where $\triangle = 1.5$ and $k = 0, ..., 17$. The true strata $y_j(\tilde{x})$ at the positions $j = 1 + \triangle k$, where $\triangle = 3$ and $k = 0, ..., 8$, are reconstructed by the proposed technique. The result of reconstruction by RWI with $LPA-ICI$ is shown in Fig.5f. The quality by both visual and numerical evaluations is significantly better then in the previous tests. It is seen that the images consist much less artefacts then obtained in Test A.

The average results for $RMSE_i$ and $PSNR_i$ values over 9 reconstructed images are presented in Table 1. The rows RI and RWI are given for the algorithms without $LPA-ICI$ filtering. The rows RI with $LPA-ICI$ and RWI with $LPA-ICI$ are given for the algorithms where $LPA-ICI$ filtering is used. It is clearly seen that RWI with $LPA-ICI$ always performs better then others and improvement over RI is approximately 1.2-1.4dB. The numerical improvement of the RWI and RWI with $LPA-ICI$ versus RI algorithms is negligible. However, visually the RWI with the $LPA-ICI$ filtering always results in the improved imaging.

Overall, the RWI algorithm always gives the best results. The images are well-denoised and the edges are better preserved. However, some minor artefacts, produced by neighboring strata, can be noticed.

A *MATLAB* implementation of the developed algorithms is available at *http://www.cs.tut.fi/~lasip/*.

5. CONCLUSIONS

Computational sectioning imaging is known to be efficient for three dimensional inverse imaging. However, the ill-conditioning of the PSF results in a high sensitivity of the inverse with respect to even small noises and disturbance. In this paper we propose a novel technique with a good potential for high-resolution $3D$ image reconstruction and efficient noise suppression. The technique is a multi-channel generalization of the algorithms for $2D$ inverse imaging developed in.[11] Efficient deconvolution algorithms in combination with a point-wise adaptive denoising make this approach powerful tool for the visualization of $3D$ objects in microscopy, astronomy, or in everyday digital photo-images.

ACKNOWLEDGMENTS

In part this work was supported by the Academy of Finland, Finnish Center of Excellence Programme 2000-2005, and EU project NoE FP6-PLT 511568-3DTV. The work of Vladimir Katkovnik was supported by a Visiting Fellow grant from Nokia Foundation.

REFERENCES

1. Schaefer L. H., Schuster D., Herz. H., "Generalized Approach for Accelerating Maximum Likelihood Based Image Restoration Applied to Three-Dimensional Fluorescence Microscopy", *Journal of Microscopy*, Vol. 204, Pt.2, pp. 99-107, Nov. 2001.
2. Preza C., Conchello J., "Depth-Variant Maximum Likelihood Restoration for Three-Dimensional Fluorescence Microscopy", *Journal of Optical Society of America A*, No. 9, Vol. 21, Sep. 2004.
3. Rajagopalan A.N., S. Chaudhuri, "An MRF Model-Based Approach to Simultaneous Recovery of Depth and Restoration from Defocused Images", *IEEE Trans. on Pattern Analysis and Amchine Intelligence*, Vol. 21, No. 7, pp. 577-589, July 1999.
4. Kubota A., Aizawa K., "Reconstructing arbitrarily focused images from two differently focused images using linear filters", *IEEE Transactions on Image Processing*, Vol. 14, Issue 11, pp. 1848 - 1859, Nov. 2005.
5. Tikhonov A. N., Arsenin V. Y., *Solutions of Ill Posed Problems,* Willey, New York, 1977.
6. Markham J., Conchello J., "Fast Maximum-Likelihood Image Restoration Algorithms for Three-Dimensional Fluorescense Microscopy", *Journal of Optical Society of America A*, 18, pp. 1062-1071, 2001.
7. McNally J., Karpova T., Cooper J., and Conchello J., "Three-dimensional imaging by deconvolution microscopy, " Methods, vol.19, pp. 373-385, 1999.

8. Zhu D., Razaz M., Lee R., "A Landweber Algorithm for 3D Confocal Microscopy Restoration", Proceedings of the 17th International Conference on Pattern Recognition, ICPR 2004, Vol. 1, Pp. 552 - 555, Aug. 2004.
9. Homem M.R.P., Mascarenhas N.D.A., Costa L da.F., 6th IEEE Southwest Symposium on Image Analysis and Interpretation, pp. 142 - 146, March 2004.
10. Forster B., Van De Ville D., Berent J., Sage D., Unser M., Extended depth-of-focus for multi-channel microscopy images: a complex wavelet approach, IEEE International Symposium on Biomedical Imaging, vol. 1, pp. 660 - 663, April 2004.
11. Katkovnik V., Egiazarian K. and Astola J., "A spatially adaptive nonparametric image deblurring," *IEEE Transactions on Image Processing*, Vol. 14, No. 10, pp. 1469-1478, October 2005.
12. Rushforth C., *Image Recovery: Theory and Application, Chap. Signal Restoration, functional analysis, and Fredholm integral eguations of the first kind.* Academis Press, 1987.
13. Li J., Agathoklis P., Peet F., Jensen G., Sahota T., Measurement and analysis of defocused point spread functions and optical transfer functions of a microscope, Proceedings of IEEE Pacific Rim Conference on Communications, Computers, and Signal Processing, 1995, pp. 407 - 410, May 1995.
14. Katkovnik V., "A new method for varying adaptive bandwidth selection", *IEEE Trans. on Signal Proc.,* vol. 47, no. 9, pp. 2567-2571, 1999.
15. Katkovnik V., K. Egiazarian, and J. Astola, *Adaptive varying scale methods in image processing,* Tampere International Center for Signal Processing, TICSP Series, no. 19, Tampere, TTY, Monistamo, 2003.
16. Katkovnik, V., A. Foi, K. Egiazarian, and J. Astola, "Directional varying scale approximations for anisotropic signal processing", Proc. XII European Signal Proc. Conf., EUSIPCO 2004, Vienna, pp. 101-104, September 2004.
17. Ng M. K., "Total Variation Based Image Restoration of Three Dimensional Microscopic Objects", *TENCON '96. Proceedings, 1996 IEEE TENCON, Digital Signal Processing Applications*, Vol. 1, 26-29, pp. 288-293, Nov. 1996
18. Goldenshluger A., and Nemirovski A., "On spatial adaptive estimation of nonparametric regression", *Math. Meth. Statistics*, vol. 6, pp. 135 – 170, 1997.
19. Foi A., Katkovnik V., Egiazarian K., and Astola J., "Inverse halftoning based on the anisotropic LPA-ICI deconvolution", In: Astola, J. et al. (eds). Proceedings of The 2004 International TICSP Workshop on Spectral Methods and Multirate Signal Processing, SMMSP 2004, Vienna, Austria, 11-12 September 2004, pp. 49 – 56, 2004.
20. Stanković L., "Performance analysis of the adaptive algorithm for bias-to-variance tradeoff", *IEEE Trans. on Signal Proc.*, vol. 52, No. 5, pp. 1228 – 1234, 2004.
21. Hampel F.R., Ronchetti E.M., Rousseeuw P.J., and Stahel W.A., *Robust Statistics, The Approach Based on Influence Functions*. Wiley: New York, 1986.
22. Donoho D.L., "De-noising by soft-thresholding", *IEEE Trans. Inform. Theory*, vol. 41, pp. 613-627, May 1995.

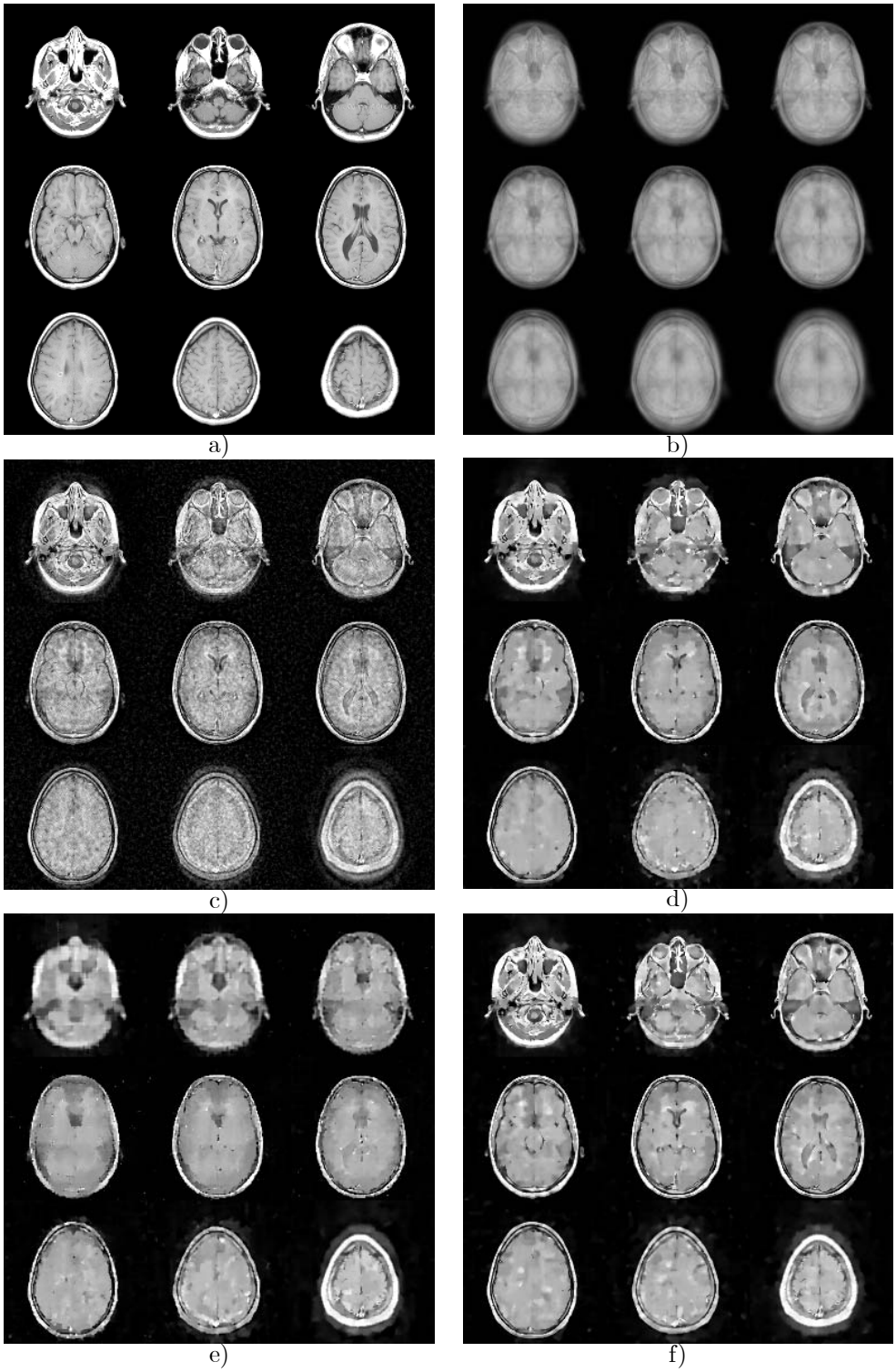

Figure 5. The reconstruction of the true MRI object: a) True object strata (j=1,4,...,26); b) Observations made by focusing at the positions of the true strata given in (a); c) RI reconstruction of (a) using observations (b); d) RWI reconsruction with $LPA-ICI$ denoising of (a) using observations (b) (Test A); e) RWI reconsruction with $LPA-ICI$ denoising of the strata (a) when the observations are made at shifted positions (Test B); f) RWI reconsruction with $LPA-ICI$ denoising of the object strata (a) when observations are made by focusing at a larger number of positions then given in (b) (Test C).